

A&A manuscript no.
(will be inserted by hand later)

Your thesaurus codes are:
06(13.19.3;08.06.2;09.11.1;09.13.2;09.01.1;02.18.7)

Modeling the millimeter emission from the Cepheus A young stellar cluster: Evidence for large scale collapse

S. Bottinelli and J. P. Williams

Institute for Astronomy, University of Hawai'i, Honolulu, HI 96822

Received / Accepted

Abstract. Evidence for a large scale flow of low density gas onto the Cepheus A young stellar cluster is presented. Observations of K-band near-infrared and multi-transition CS and N₂H⁺ millimeter line emission are shown in relation to a sub-millimeter map of the cool dust around the most embedded stars. The near-infrared emission is offset from the dust peak suggesting a shift in the location of star formation over the history of the core. The CS emission is concentrated toward the core center but N₂H⁺ peaks in two main cores offset from the center, opposite to the chemistry observed in low mass cores. A starless core with strong CS but weak N₂H⁺ emission is found toward the western edge of the region. The average CS(2–1) spectrum over the cluster forming core is asymmetrically self-absorbed suggesting infall. We analyze the large scale dynamics by applying a one-dimensional radiative transfer code to a model spherical core with constant temperature and linewidth, and a density profile measured from an archival 850 μm map of the region. The best fit model that matches the three CS profiles requires a low CS abundance in the core and an outer, infalling envelope with a low density and undepleted CS abundance. The integrated intensities of the two N₂H⁺ lines is well matched with a constant N₂H⁺ abundance. The envelope infall velocity is tightly constrained by the CS(2–1) asymmetry and is subsonic but the size of the infalling region is poorly determined. The picture of a high density center with depleted CS slowly accreting a low density outer envelope with normal CS abundance suggests that core growth occurs at least partially by the dissipation of turbulent support on large scales.

Key words: Radio lines: ISM – Stars: formation – ISM: kinematics and dynamics – ISM: molecules – ISM: abundances – Radiative transfer

1. Introduction

Most stars, particularly massive stars, form in groups (e.g. Carpenter 2000). It is therefore essential to study cluster forming regions in order to understand more completely the way in which the majority of stars are formed. Isolated low mass star formation occurs via the nearly isothermal free-fall collapse of a dense molecular cloud core, followed by the evolutionary phases Class 0, I, II and III objects (e.g. Evans 1999). However, the applicability of this paradigm to the formation of massive stars is debated (Garay & Lizano 1999): for example, massive stars begin burning hydrogen and reach the main sequence while still accreting matter from the surrounding protostellar envelope and they can also develop strong winds, both of which will strongly affect the physical conditions, structure and chemistry of their surroundings. Due to the shape of the IMF and the fact that they evolve faster, massive protostars are rarer (and therefore more distant on average) than low mass protostars. Consequently fewer Class 0 massive protostar counterparts have been studied in detail. It is only recently that catalogs of high-mass protostellar objects have been made (e.g. Sridharan et al. 2002).

The molecular cloud core Cepheus A East (hereafter Cep A) is a nearby site of massive star formation (Sargent 1977) located in the Cepheus OB association at a distance of 725 pc (Blauuw et al. 1959). The far-IR luminosity is $2.4 \times 10^4 L_{\odot}$ (Evans et al. 1981), corresponding to a small cluster of B stars. Cep A harbors one of the first molecular bipolar outflow sources discovered (Rodríguez et al. 1980). Higher spatial resolution CO observations showed the outflow to be extremely complex, and it was termed quadrupolar (Torrelles et al. 1993). The fastest components of this outflow are bipolar and oriented northwest-southeast (Rodríguez et al. 1980), perpendicular to the low velocity CO structure. The slower and more extended component has been interpreted as the diverting and redirecting of the main outflow by the interaction with interstellar high-density gas, seen in NH₃ lines by Torrelles et al. (1993). Ultra compact H II regions and a diffuse thermal dust emission source have been identified

from 20 μm maps and 6 cm low-resolution VLA observations by Beichman et al. (1979). Seven ionized hydrogen complexes lie in “strings” that form a “Y” tilted to the east (Hughes & Wouterloot 1984), the bifurcation point of which is coincident with the exciting source of the molecular outflow. A cluster of compact radio sources have been identified as pre-main-sequence stars by Hughes (1988) due to their variability and the presence of OH and H_2O maser emission. From subsequent ammonia VLA observations, Torrelles et al. (1993) proposed that one of these radio sources, HW2, is a $\sim 10\text{--}20 M_\odot$ protostar. The larger core surrounding the cluster has temperature 35 K and mass $200 - 300 M_\odot$ Moriarty-Schieven et al. (1991). On the basis of its protostellar content, high luminosity and low temperature, and following the bolometric temperature definition of Chen et al. (1995), the Cep A core may be considered a high mass Class 0 source.

In order to examine the properties of this young, massive cluster forming region, we obtained near-infrared and millimeter wavelength multi-transition CS and N_2H^+ data. The observations are discussed in §2. We derive the density profile from 850 μm continuum measurements and fit core-averaged spectra using a 1-D radiative transfer model in §3. Our results indicate large CS depletion in the central core and an outer undepleted accreting layer. We discuss these results and conclude in §4.

2. Observations

2.1. Millimeter Data

Observations were made with the 10 antenna Berkeley-Illinois-Maryland array¹ (BIMA) for two 8 hour tracks in CS(2–1) in April and May 1998 and one 8 hour track in $\text{N}_2\text{H}^+(1\text{--}0)$ in May 1998, all in C-array. A seven field hexagonal mosaic was made with phase center, $\alpha(2000) = 22^{\text{h}}56^{\text{m}}18^{\text{s}}.9$, $\delta(2000) = 62^\circ 01' 42''.6$. Amplitude and phase were calibrated using 5 minute observations of 2322+509 interleaved with each 25 minute integration on source. The calibrator flux was 0.66 ± 0.22 Jy based on observations of Uranus during the middle of each track. The correlator was configured with two sets of 256 channels at a bandwidth of 12.5 MHz (0.15 km s^{-1} per channel) in each sideband and a total continuum bandwidth of 800 MHz. Data reduction was carried out using standard procedures in the MIRIAD package. The final maps covered a hexagonal region $\sim 3'.5 \times 3'.5$ region at $\sim 9'' \times 7''$ resolution.

Complementary single-dish maps of the same lines were made at the Five College Radio Astronomy Observatory² (FCRAO) 14 m telescope in December 1999 using

the SEQUOIA 16 beam array receiver and the FAAS backend consisting of 15 autocorrelation spectrometers with 1024 channels set to an effective resolution of 24 kHz (0.06 km s^{-1}). The CS and N_2H^+ lines were observed simultaneously in frequency switching mode. The pointing and focus were checked every three hours on nearby SiO maser sources. Third order baselines were removed from the data and spectra coadded using the CLASS package. The resolution of the data is $50''$ and the final maps were Nyquist sampled over $8' \times 8'$ centered on the BIMA phase center. A single spectrum of $\text{C}^{34}\text{S}(2\text{--}1)$ was also taken toward the map center using the same setup.

The FCRAO data were combined with the BIMA data using maximum entropy deconvolution (using a gain for FCRAO at these frequencies of 43.7 Jy K^{-1}). The resulting maps show the large scale structure observed in the single-dish map at the $\sim 10''$ resolution of the interferometer map. These maps have an rms noise of 0.2 and 0.4 K per 0.5 km s^{-1} channel, for CS (2–1) and $\text{N}_2\text{H}^+(1\text{--}0)$ respectively. All the flux is recovered in the combined map but features at intermediate scales, in the range $70''\text{--}100''$, may be poorly represented (e.g. Williams et al. 2003).

Observations of CS(5–4), CS(7–6) and $\text{N}_2\text{H}^+(3\text{--}2)$ were made at the Heinrich Hertz Telescope³ (HHT) in November 1999. The data were taken using the SIS-230 and SIS-345 receivers and AOS backend (2048 channels, 48 kHz resolution) in on-the-fly (OTF) mode. Pointing and focus were checked using observations of Saturn and Orion IRc2. The final maps, made from several OTF maps in orthogonal scan directions, were coadded and first order baselines removed using the CLASS package. The resolution of the observations is $31''$, $22''$, and $27''$ for CS(5–4), CS(7–6) and $\text{N}_2\text{H}^+(3\text{--}2)$ respectively and the final maps covered $3'.5 \times 3'.5$, with an rms noise of 0.4 K per 0.5 km s^{-1} channel.

To compare the near-infrared and millimeter wavelength line data with the cool dust emission around the most embedded (Class 0 counterpart) stars in the cluster, we downloaded archival SCUBA observations taken on the James Clerk Maxwell Telescope in August 1997 and reduced them using the SURF package.

2.2. Infrared Data

Cep A was observed on the University of Hawai'i 2.2m telescope at the f/10 focus with QUIRC (QUick InfraRed Camera) in K band ($2.200 \mu\text{m}$) in July and August 2003. The plate scale of the telescope is $0.1886 \text{ arcsec pixel}^{-1}$ and the field-of-view $193'' \times 193''$. The total on source integration time was 23.2 minutes. The average seeing was

¹ The BIMA array is operated with support from the National Science Foundation under grants AST-9981308 to UC Berkeley, AST-9981363 to U. Illinois, and AST-9981289 to U. Maryland.

² FCRAO is supported in part by the National Science Foundation under grant AST-0100793 and is operated with permis-

sion of the Metropolitan District Commission, Commonwealth of Massachusetts.

³ The HHT is operated by the Submillimeter Telescope Observatory on behalf of Steward Observatory and the Max-Planck-Institut fuer Radioastronomie.

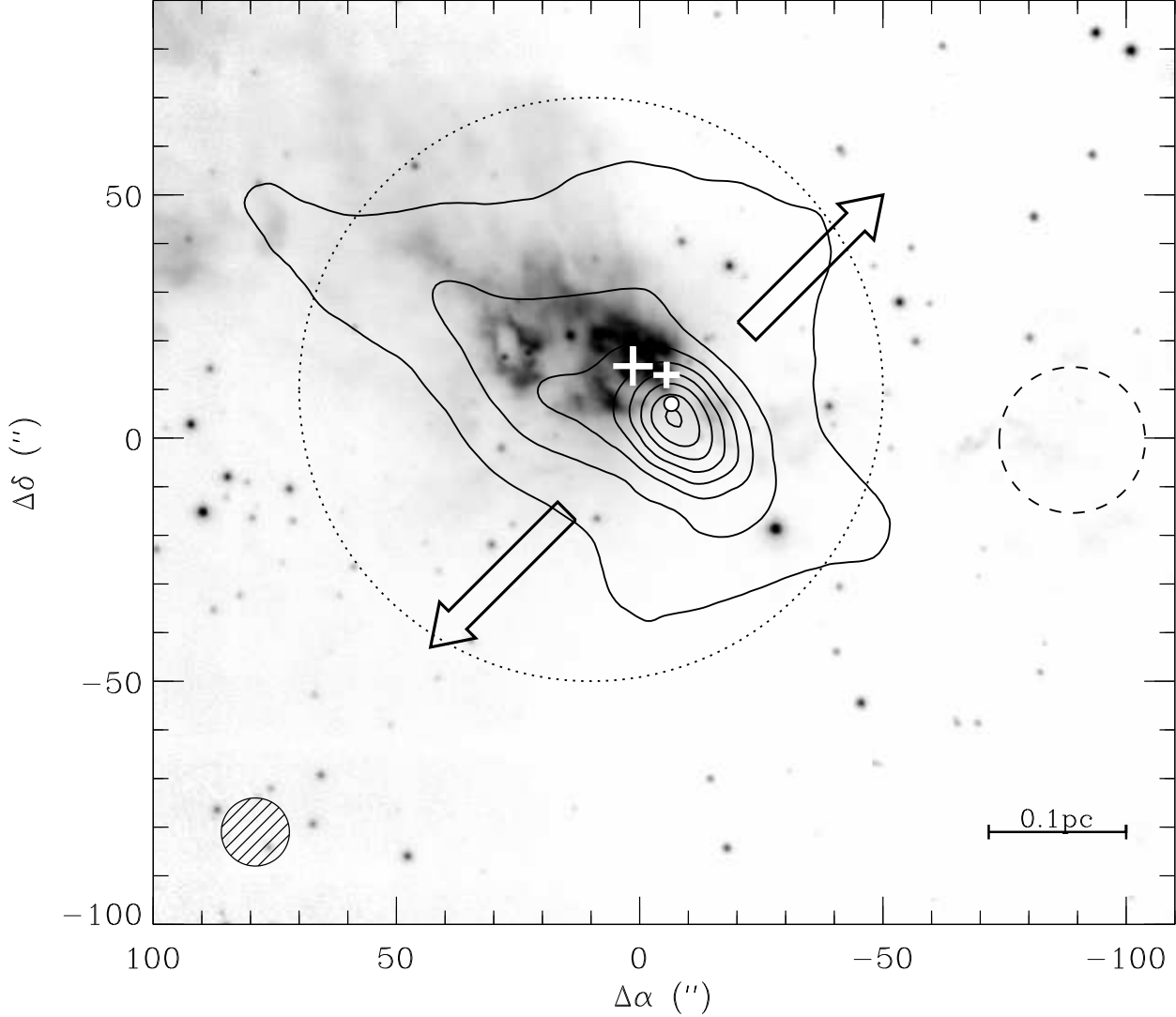


Fig. 1. Grayscale K-band image over-plotted with SCUBA 850 μm contours of Cep A showing the stellar and dust content. The central position is at $\alpha(2000) = 22^{\text{h}}56^{\text{m}}18^{\text{s}}.9$, $\delta(2000) = 62^{\circ}01'42''.6$. The 850 μm contours start at 1 Jy beam^{-1} and increment by 2 Jy beam^{-1} . The large and small white plus signs show the location of the IRAS and MSX point sources respectively (each with a positional accuracy of less than $5''$). The small white circle near the center of the map marks the location of the high mass protostar, HW2. The arrows show the direction of the bipolar CO outflow observed by Rodríguez et al. (1980). The dashed circle at the western edge of the map shows the location of the starless core seen in the CS maps and the dotted circle, centered at (10,10) with diameter $2'$ defines the region over which the spectral line averages were calculated.

$1''.1$ FWHM. The observations were carried out by taking alternate object and sky exposures. All frames were flat-fielded using a normalized incandescent light dome flat. Sky frames were obtained by computing the median of several sky exposures close in time to a given object frame. The sky frames were subtracted from the object frames. The individual images were registered and co-added to

produce a single image. Unfortunately, the conditions were non-photometric but we conservatively estimate that we should be able to detect to a limiting magnitude of at least 19, which is 3.4 magnitudes fainter than 2MASS.

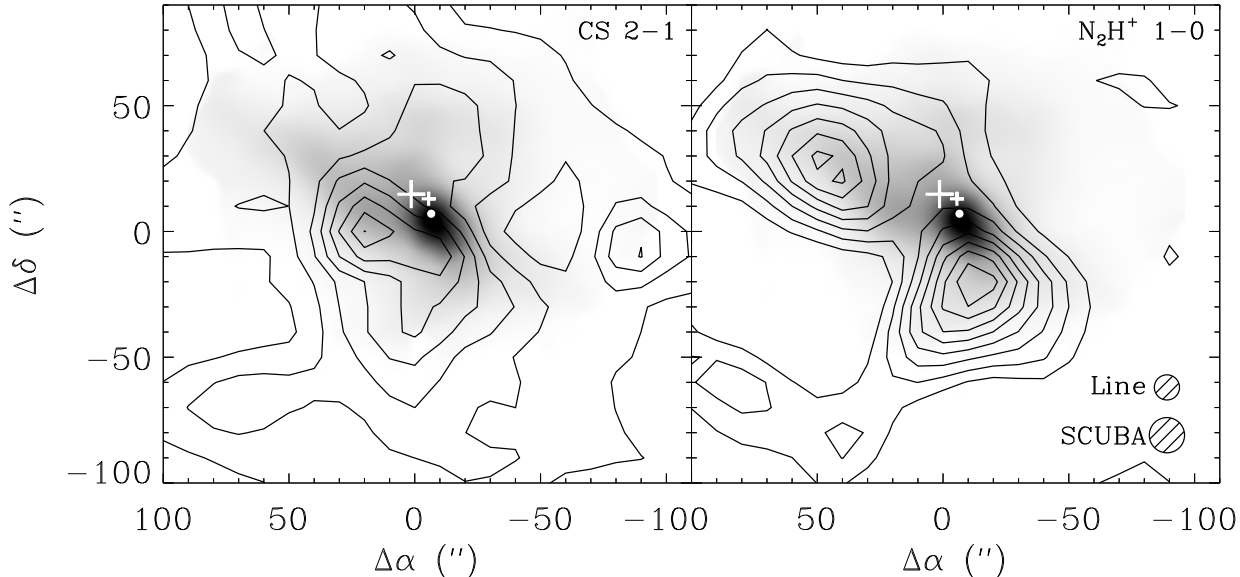


Fig. 2. Comparison of line and dust emission. The line maps have a resolution of $10''$ and are contoured with starting levels and increments equal to 4.0 K km s^{-1} for CS (2–1) and 5.0 for N_2H^+ (1–0). The dust emission has a resolution of $14''$ and is shown as a grayscale ranging from 1 to 15 Jy beam^{-1} . Symbols are as in Figure 1.

3. Analysis

3.1. Continuum and Line Maps

Figure 1 shows contours of the $850 \mu\text{m}$ continuum emission overlaid on the grayscale K-band image. Note that for 35 K dust and the SCUBA beamsize of $14''$, 1 Jy beam^{-1} corresponds to a visual extinction, $A_V = 24$, or an extinction at K-band, $A_K = 2.4$. The infrared nebulosity lies within the extended sub-millimeter emission ($A_K \sim 5 - 8$) but is offset from the peak. There is one IRAS and one MSX point source in the region, slightly offset from each other. The IRAS-HiRes $12 \mu\text{m}$ and MSX $10 \mu\text{m}$ emission are both associated with the near-infrared nebulosity, but the $60 \mu\text{m}$ IRAS-HiRes image peak is closer to the maximum of the $850 \mu\text{m}$ map, which traces the cooler dust. This suggests a spread in ages and location of star formation in Cep A, with the youngest protostars more deeply embedded in the core and invisible at near- and mid-infrared wavelengths.

Spectral line maps and their comparison with the dust emission are shown in Figures 2, 3. In each case the emission has been integrated over the full extent of the line, including all hyperfine components in the case of N_2H^+ . Figure 2 shows the combined BIMA+FCRAO data at $10''$ resolution. Figure 3 shows these maps and the higher transition data smoothed to a uniform resolution of $30''$. Due to their high dipole moments, CS and N_2H^+ both trace high volume densities over a range, $n_{\text{H}_2} \sim 10^4 - 10^6 \text{ cm}^{-3}$, for these transitions. The complex structure apparent in the line maps contrasts with the relative simplicity

of the dust continuum emission. The spatial distribution of N_2H^+ is similar to that of the ammonia (Torrelles et al. 1993) and generally follows the $850 \mu\text{m}$ continuum emission, but N_2H^+ is notably absent toward the core center where the CS is strongest. This behavior is opposite to the situation in low mass cores where N_2H^+ is more centrally concentrated than CS (Tafalla et al. 2002).

The maps also reveal an apparently starless core located $\sim 90''$ to the west of the bright $850 \mu\text{m}$ peak, indicated by a cross on Figure 1. The core is detected in CS(2–1) and (5–4) but has only very weak N_2H^+ (1–0) emission (Figure 2) and no stars are seen in the near-infrared image. This core is on the edge of the SCUBA map where there is extended emission but no significant peak. The presence of CS (5–4) emission indicates large enough densities that we would expect to observe N_2H^+ emission, as in the large core. Since this emission is very weak, there must be a variation of abundances between the two cores. Potential reasons for the wide range of abundances throughout the region are discussed in §4.

3.2. Radiative Transfer Modeling

Our understanding of the structure and dynamics in Cep A is complicated by the small scale chemical variations within the core. Henceforth, we restrict attention to the large scale properties of the region as if observed with a $2'$ gaussian beam centered at offset (10,10). The size and location of the averaging region was chosen so as to be broadly centered on the sub-millimeter continuum map

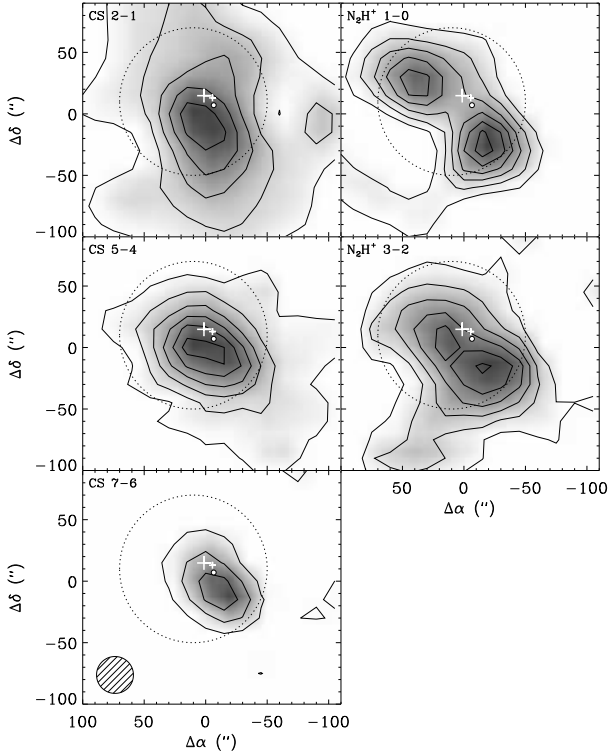


Fig. 3. Line maps of the Cepheus A core shown as grayscale with contours overlaid. Positions are given in offset coordinates with the same central position as Figure 1. CS maps are shown in the left panels and N_2H^+ in the right. The maps have been smoothed to a uniform $30''$ resolution. The contour starting levels and increments for each map are 4.0 K km s^{-1} (CS 2–1), 4.0 (CS 5–4), 1.5 (CS 7–6), 5.0 (N_2H^+ 1–0), and 3.0 (N_2H^+ 3–2). Note the isolated core in the CS(2–1) map $\sim 90''$ west of center (see text for discussion). The $2'$ diameter circle shows the region over which the data were averaged to analyze the large scale dynamics of the core, and symbols are as in Figure 1.

but also to include the most prominent CS and N_2H^+ structures within the core. The averaging region is indicated on the continuum and line maps in Figures 1 and 3. Averaged line profiles are displayed in Figure 4. This figure also includes the line profile for $\text{C}^{34}\text{S}(2-1)$. This isotopomer of CS, which is less abundant and therefore optically thinner, peaks near the same velocity as the dip in the average CS(2–1) spectrum. We therefore conclude that the two peaks in the latter are due to radiative effects (self-absorption) and not two features along the line of sight. Although individual CS profiles show both blue- and red-shifted self-absorption that may be due to a mix of infall, outflow, and rotation (Di Francesco et al. 2001), the average CS(2–1) profile has a blue-shifted peak brighter than

the red-shifted one, indicating that infall is the dominant effect on the scale of the core (Leung & Brown 1977).

In order to examine the properties of the large scale structure and dynamics, we modeled the core average line profiles using the radiative transfer code, *ratran* (Hogerheijde & van der Tak 2000). Collisional rate coefficients for CS are from Turner et al. (1992) and for N_2H^+ from Monteiro (1985 and references therein). From the brightness temperature of the N_2H^+ and assuming an excitation temperature equal to the dust temperature, 35 K, we estimate the optical depth of each hyperfine component to be less than 0.1. For the purposes of the modeling, therefore, we can ignore the complicated hyperfine structure (7 components at $J = 1-0$ and 45 at $J = 3-2$) and simply match the integrated intensity of each rotational transition.

The inputs to the radiative transfer model include the density, temperature, and velocity structure of the core and the abundances of each molecule. However, many parameters are constrained by related observations and results. The remaining free parameters, eight in all, were then varied so as to fit the profiles of each of the three CS transitions and the integrated intensity of the two N_2H^+ transitions.

3.2.1. Model inputs

The $850 \mu\text{m}$ map in Figure 1 allows us to measure the column density profile of the core and thereby estimate the volume density. Since the radiative transfer model is one-dimensional, we approximated the density structure as a radial function by calculating the average flux in concentric elliptical annuli centered on the peak of the emission. The equivalent radii were defined as the geometric mean of the semi-major and semi-minor axes of each ellipse. The column density was determined by assuming a dust temperature of 35 K (Moriarty-Schieven et al. 1991) and a mass-opacity $\kappa = 0.02 \text{ cm}^2 \text{ g}^{-1}$ (Ossenkopf & Henning 1994). The volume density was then derived by assuming a path length through the core equal to twice the equivalent radius. The resulting density profile was fit to a Plummer-like model,

$$n_{\text{H}_2}(r) = n_0 \left[1 + \left(\frac{r}{r_0} \right)^2 \right]^{-\alpha/2},$$

where $n_0 = 1.1 \times 10^7 \text{ cm}^{-3}$, $r_0 = 0.02 \text{ pc}$ and $\alpha = 2.0$. The model discretizes this density profile over nine logarithmically spaced shells. Both measured and discretized density profiles are displayed in Fig. 5; there are no data points for radii smaller than 0.03 pc , the equivalent radius corresponding to a semi-minor axis of half the $850 \mu\text{m}$ beam-size, and for radii larger than 0.18 pc , which corresponds to the extent of the $850 \mu\text{m}$ map.

Additional inputs to the model include a temperature of 35 K, derived from a graybody fit to the SED

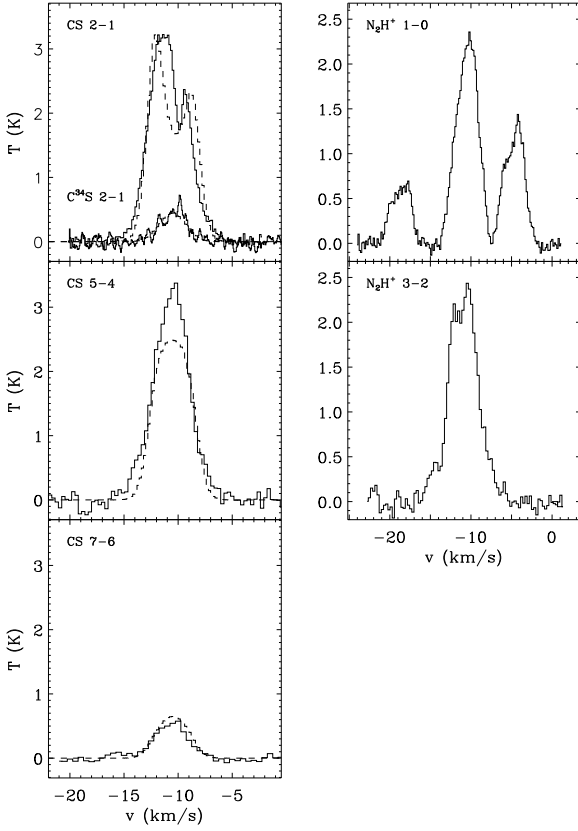


Fig. 4. Averages of CS and $C^{34}S$ (2–1) (left) and N_2H^+ (right) spectra over the central core region outlined by the circles in Figures 1 and 3. The heavy solid lines show the observed data and the dashed line shows the modeled profiles for the CS lines. The multiple peaks in the N_2H^+ spectra is due to hyperfine structure which was not modeled (the fits matched only the integrated intensity of each rotational transition).

(Moriarty-Schieven et al. 1991), and a systemic velocity and velocity dispersion derived from fitting the optically thin $N_2H^+(1-0)$ line, $v_{\text{core}} = -10.5 \text{ km s}^{-1}$ and $\sigma_{\text{core}} = 1.2 \text{ km s}^{-1}$, respectively. A constant temperature and velocity dispersion were adequate to model the core.

To model the observed self-absorption in the CS(2–1) line, we found that we required a low excitation (and therefore low density) and low velocity dispersion ($\sigma_{\text{env}} = 1.1 \text{ km s}^{-1}$) outer shell. The low velocity dispersion is required by the narrowness of the observed absorption dip. The overall model has 10 shells therefore, but it can effectively be considered as two layers; a power law core on the inside and a low density outer envelope. The free parameters in the model are the inner core cutoff radius, the size, density, velocity dispersion and relative velocity of the envelope and the molecular abundances in the core and envelope.

The values for the molecular abundances were guided by observations of other cores and theoretical mod-

els. In cold molecular cloud cores prior to star formation, the chemistry is dominated by low-temperature gas-phase ion-molecule and neutral-neutral reactions (van Dishoeck & Blake 1998). During the cold collapse phase, however, the density becomes so high that many molecules freeze onto grain surfaces. Tafalla et al. (1998) find that, in low mass star forming cores, the abundances of the tightly bound sulfur-bearing molecules such as CS begin to exhibit large depletions at densities in the range, $n_{H_2} \sim 2 - 6 \times 10^4 \text{ cm}^{-3}$. This behavior is in contrast to that of N_2H^+ which, due to the low binding energy of the precursor molecule N_2 , depletes only at the highest densities (Bergin & Langer 1997). Based on these results, we assume a constant abundance of N_2H^+ but allow the CS abundance to vary. As we show later, we fit the data with a simple “jump” model where the CS is depleted in the inner dense core relative to a lower density outer envelope. This is a similar abundance profile to the detailed chemical modeling of the high mass star forming region, AFGL 2591, by Doty et al. (2002).

3.2.2. Model results

By varying the density, size and velocity of the envelope, and the CS abundance in the core and envelope, we were able to fit the integrated intensities of the three observed CS transitions to within 20% and reproduce the asymmetry in the (2–1) line reasonably well. The observed and model CS spectra are compared in Figure 3. The parameters of the fit are tabulated in Table 1, where r_{core} is the inner core cut-off radius, r_{env} , n_{env} and $v_{\text{in}} = v_{\text{env}} - v_{\text{core}}$ are the size, density and relative velocity of the outer envelope, and $x(\text{CS})_{\text{core}}$ and $x(\text{CS})_{\text{env}}$ are the CS abundances in the core and the envelope respectively. The density, velocity, and CS abundance profiles are graphed in Figure 5 and annotated with the above parameters. Simultaneously, the $N_2H^+(1-0)$ and (3–2) integrated intensities were also matched: we found 8.1 and 9.5 K km s^{-1} respectively for the modeled values, whereas the observed values are 9.7 and 8.2 K km s^{-1} for the (1–0) and (3–2) transitions respectively. These results correspond to a match of 16 and 15% respectively. Finally, we also fitted the $C^{34}S$ (2–1) integrated intensity, using an abundance $x(C^{34}S) = x(\text{CS})/30$. We found a modeled value of 1.4 K km s^{-1} which is within 8% of the observed value (1.5 K km s^{-1}).

Despite the good overall fit, some slight discrepancies remain. The observed CS(5–4) is stronger than the model by 20%. This may be due to calibration error or may reflect a more complex CS abundance profile in the core. The observed CS(2–1) profile is slightly narrower than the model spectrum, perhaps due to the constant linewidth assumption in the core (the velocity dispersion of cores is expected to decrease with radius, Larson 1981). A more refined model with additional parameters would fit the data more closely but probably not with greater significance.

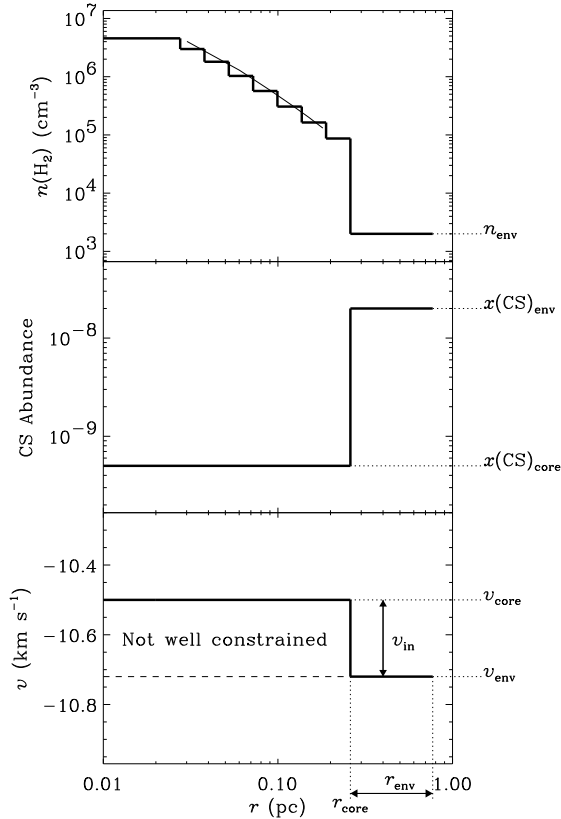


Fig. 5. Radial profiles of H_2 volume density, core-envelope CS abundance and velocity profiles used in the best fit model. Relative motions in the inner region, $r < r_{\text{core}}$, were not well constrained by the data. The thin solid line shows the H_2 density profile derived from the $850 \mu\text{m}$ data (see text).

Since the model reproduces the blue-red asymmetry in the CS(2–1) spectrum well we are confident that we have accurately measured the average infall speed of the envelope, $v_{\text{in}} = -0.22 \text{ km s}^{-1}$. However, the size of the infalling region is not well determined because the average profiles of the higher transition CS lines are not self-absorbed and therefore relative motions of the higher density gas could not be constrained. Nevertheless, we were unable to model the spectra with a static outer shell and an inner collapse: no such set of parameters could reproduce the dip in the CS (2–1) spectrum. That is, our results indicate a *large scale collapse from the outside-in*.

4. Discussion and Summary

The line observations reveal a complex chemistry in the core. The CS emission is concentrated toward the center near the peak of the $850 \mu\text{m}$ dust emission and the youngest, most embedded protostars. However, the N_2H^+ map shows two prominent cores offset on either side of the dust peak. The presence of CS and absence of N_2H^+ to-

Table 1. Fit parameters.

Parameter	Value
r_{core}	0.26 pc
r_{env}	0.51 pc
n_{env}	$2 \times 10^3 \text{ cm}^{-3}$
σ_{env}	1.1 km s^{-1}
v_{in}	-0.22 km s^{-1}
$x(\text{CS})_{\text{core}}$	5×10^{-10}
$x(\text{CS})_{\text{env}}$	2×10^{-8}
$x(\text{N}_2\text{H}^+)$	3×10^{-11}

ward the star forming center of the core is likely due to the fact that neutral molecules released from the dust grains in the hotter region surrounding the protostars preferentially destroy ions such as N_2H^+ (Bergin 2000).

The maps also reveal a small starless core toward the west of the main core. The relatively strong CS and weak N_2H^+ emission toward this core suggests that it has only recently formed (Bergin & Langer 1997). Williams & Myers (1999) found a starless core with similar chemical properties in the Serpens NW cluster

Despite the chemical complexities on small scales, the average CS(2–1) spectrum is asymmetrically self-absorbed suggesting large scale collapse. Using the Hogerheijde & van der Tak radiative transfer code, we fit the average CS and N_2H^+ spectra with a spherical model consisting of an inner region with a Plummer-like density profile measured from archival SCUBA $850 \mu\text{m}$ data with constant temperature and linewidth. The best fit model that matches the three CS profiles has a low CS abundance in the inner region and an outer, infalling envelope with a low density and higher CS abundance. The depletion toward the center matches chemical evolution model expectations (Bergin & Langer 1997) and the envelope CS abundance is similar to that in the extended ridge of Orion (van Dishoeck & Blake 1998). The fit also matched the integrated intensities of the two N_2H^+ spectra with a constant abundance similar to that found in B68 (Bergin et al. 2002). In practice the maps show that the N_2H^+ must deplete toward the core center (see also Doty et al. 2002) but we have not attempted to match the complicated small scale chemistry and our model fit for the N_2H^+ abundance should only be considered an average, weighted by column density, over the core.

The CS(2–1) self-absorption requires a large scale outside-in collapse. The velocity of the collapse could be accurately measured but the depth of the collapse region could not, due to the absence of self-absorption in the higher transition CS lines. At 0.22 km s^{-1} , the infall velocity is sub-sonic for a gas temperature of 35 K. The mass infall rate of the envelope can be estimated from the ratio of its mass, $M_{\text{env}} = 240 M_{\odot}$ determined from its size and density, and the time for the outer edge to reach the core

center,

$$\dot{M}_{\text{in}} = \frac{M_{\text{env}} v_{\text{in}}}{r_{\text{env}} + r_{\text{core}}} = 7 \times 10^{-5} M_{\odot} \text{yr}^{-1}.$$

This may only be a lower limit to the total mass infall rate at the center if the inner region is also collapsing. Nevertheless, the envelope mass infall rate alone is more than an order of magnitude higher than typical mass infall rates for solar mass protostars (Zhou 1995).

Our data do not rule out inside-out collapse motions around individual protostars at higher densities on smaller size scales since the $\tau = 1$ surface of the CS(2–1) emission occurs at low densities and therefore at large scales. The multitude of sources, powerful outflows, and the complex chemistry would likely make an investigation of the small scale motions around individual protostars quite challenging.

On large scales, however, our picture is of a core with a Plummer-like density profile accreting low density gas sub-sonically. The CS abundance in the infalling envelope is similar to undepleted values in the ISM. The dissipation of turbulent support resulting in “cooling flows” may lead to core growth in this manner (Nakano 1998 ; Myers & Lazarian 1998 ; Williams & Myers 2000). The growing availability of dust continuum maps and multi-transition, multi-species line observations will lead to more refined structural and dynamical modeling and comparisons between different star forming environments in the future.

Acknowledgements. This work began when JPW was a Jansky fellow and he thanks the NRAO for their support. The more recent analysis was supported by NSF grant AST-0324328. We thank Harold Butner for assistance with the observations at the Heinrich Hertz Telescope, Ted Bergin, Eric Herbst and Phil Myers for informative discussions, and the referee, Gary Fuller, for useful suggestions that improved the paper.

References

Beichman, C. A., Becklin, E. E., & Wynn-Williams, C. G. 1979, *ApJ*, 232, L47
 Bergin, E.A. & Langer, W.D. 1997, *ApJ*, 486, 316
 Bergin, E.A., Melnick, G.J., & Neufeld, D.A. 1998, *ApJ*, 499, 777
 Bergin, E.A. in *Astrochemistry: From Molecular Clouds to Planetary Systems*, Proceedings of IAU Symposium 197, Y.C. Minh & E.F. van Dishoeck (eds), 2000, p.51.
 Bergin, E.A., Alves, J., Huard, T., & Lada, C. J. 2002, *ApJ*, 570, L101
 Blauuw, A., Hiltner, W.A., & Johnson, H. L. 1959, *ApJ*, 130, 69
 Carpenter, J.M. 2000, *AJ*, 120, 3139
 Chen, H., Myers, P.C., Ladd, E.F., & Wood, D.O.S. 1995, *ApJ*, 445, 377
 Di Francesco, J., Myers, P.C., Wilner, D.J., Ohashi, N., & Mardones, D. 2001, *ApJ*, 562, 770
 Doty, S.D., van Dishoeck, E.F., van der Tak, F.F.S., & Boonman, A.M.S. 2002, *A&A*, 389, 446

Evans II, N. J., Becklin, E. E., Beichman, C., Gatley, I., Hildebrand, R. H., Keene, J., Slovak, M. H., Werner, M. W., Whitcomb, S. E. 1981, *ApJ*, 244, 115
 Evans II, N.J. 1999, *ARAA*, 37, 311
 Garay, G. & Lizano, S. 1999, *PASP*, 111, 1049
 Hogerheijde, M.R. & van der Tak, F.F.S. 2000, *A&A*, 362, 697
 Hughes, V. A. & Wouterloot, J. G. A. 1984, *ApJ*, 276 204
 Hughes, V. A. 1988, *ApJ*, 333, 788
 Larson, R. B. 1981, *MNRAS*, 194, 809
 Leung, C.M., & Brown, R.B. 1977, *ApJ*, 214, L73
 Monteiro, T.S. 1985, *MNRAS*, 214, 419
 Moriarty-Schieven, G.H., Snell, R.L., & Hughes, V.A. 1991, *ApJ*, 374, 169
 Myers, P.C. & Lazarian, A. 1998, *ApJ*, 507, L160
 Nakano, T. 1998, *ApJ*, 494, 587
 Ossenkopf, V. & Henning, T. 1994, *A&A*, 291, 943
 Rodríguez, L. F., Ho, P. T. P., & Moran, J. M. 1980, *ApJ*, 240, L149
 Sargent, A.I. 1977, *ApJ*, 218, 736
 Sridharan, T.K., Beuther, H., Schilke, P., Menten, K.M., & Wyrowski 2002, *ApJ*, 566, 931
 Tafalla, M., Mardones, D., Myers, P.C., Caselli, P., Bachiller, R., & Benson, P.J. 1998, *ApJ*, 504, 900
 Tafalla, M., Myers, P.C., Caselli, P., Walmsley, C.M. & Comito, C. 2002, *ApJ*, 569, 815
 Torrelles, J. M., Verdes-Montenegro, L., Ho, P.T.P., Rodríguez, L. F., & Cantó, J. 1993, *ApJ*, 410, 202
 Turner, B.E., Chan, K.-W., Green, S., & Lubowich, D.A. 1992, *ApJ*, 399, 114
 van Dishoeck, E.F. & Blake, G.A. 1998, *ARAA*, 36, 317
 Williams, J.P. & Myers, P.C. 1999, *ApJ*, 518, L37
 Williams, J.P. & Myers, P.C. 2000, *ApJ*, 537, 891
 Williams, J.P. Plambeck, R.L., & Heyer, M.H. 2003, *ApJ*, 591, 1025
 Zhou, S. 1995, *ApJ*, 442, 685